An *ab Initio* Study of the Kinetics of the Reactions of Halomethanes with the Hydroxyl Radical. 1. CH_2Br_2

Florent Louis,* Carlos A. Gonzalez,* Robert E. Huie, and Michael J. Kurylo

Physical and Chemical Properties Division, National Institute of Standards and Technology, Gaithersburg, Maryland 20899

Received: March 24, 1999; In Final Form: January 20, 2000

Ab initio calculations were carried out with Møller−Plesset second- and fourth-order perturbation theory (MP2 and MP4), and the coupled cluster method, CCSD(T), on the H atom abstraction reaction from dibromomethane by hydroxyl radical attack. Geometry optimization and vibrational frequency calculations at the MP2 level were performed on reactants, products, and the transition state using the 6-311G(d,p) and 6-311G(2d,2p) basis sets. The geometry parameters optimized at the MP2/6-311G(2d,2p) level of theory were used in single-point energy calculations with increasing basis set sizes, from 6-311G(2d,2p) to 6-311++G-(3df,3pd) at both the MP2 and MP4(SDTQ) levels of theory. Canonical transition-state theory was used to predict the rate constants as a function of the temperature (250−400 K). It was found that the kinetic parameters obtained in this work with the spin-projected method PMP4(SDTQ)/6-311++G(3df,3pd)//MP2/6-311G(2d,-2p) are in reasonable agreement with the experimental values. The prospect of using relatively low level *ab initio* electronic structure calculations aimed at the implementation of inexpensive semiquantitative "screening tools" that could aid scientists in predicting the kinetics of similar processes is also discussed.

Introduction

In this paper, we initiate a systematic study of the application of *ab initio* electronic structure calculations combined with transition-state theory to the kinetics of hydrogen atom abstractions by hydroxyl radicals. This work is part of an ongoing effort at the National Institute of Standards and Technology (NIST) leading to the implementation of efficient and reliable computational chemistry "screening tools" useful in predicting the fate of haloalkanes once they are released into the atmosphere. Our focus is mainly directed to the use of computationally inexpensive *ab initio* molecular orbital methodologies that could be used on a routine basis by both experimentalists and computational chemists so that a reliable semiquantitative picture of the kinetics of these reactions can be obtained with the minimum amount of effort. In this work, we report results for the reaction

$$OH + CH_2Br_2 \rightarrow H_2O + CHBr_2 \qquad (R1)$$

We have chosen this reaction as a prototype of processes for which the proposed screening tool will be used. One of the reasons for this choice is the availability of reliable experimental data and because the significant computational difficulty in treating relatively large electronic systems containing bromine atoms makes this reaction a serious test of the applicability of the current quantum chemistry methodologies in such systems. Thus, it is expected that a viable theory level for this reaction should be adequate for other haloalkanes containing bromine or lighter halogen atoms. In addition, bromine is an active agent in fire suppression and inhibition.[1] In the screening for suitability as a fire suppressant, the reactivity of the agent is of important consideration, with regard to both its utility and its environmental acceptability.

* To whom Correspondence should be addressed. Fax: (301) 975−3672. E-mail: (F.L.) flouis@nist.gov, (C.A.G.) carlos.gonzalez@nist.gov.

There have been some early applications of transition-state theory to the reactions of OH with haloalkanes, making use of thermochemical kinetic tools, which provided estimates of the Arrhenius preexponential factors.[2,3] A few *ab initio* studies also have been carried out on the reactions of hydroxyl radicals with halogen-substituted methanes[4−6] or ethanes.[7−11] None of these, however, have included bromine-substituted methanes. In addition, there have been several *ab initio* studies on the reactions of fluorine and chlorine atoms with halogenated methanes[12−14] and ethanes[15,16] plus one on methyl radical reactions with halomethanes,[17] and a theoretical study of the enthalpies of formation of fluoromethanes.[18] Recently, two *ab initio* studies dealing with the structures, vibrational frequencies, thermodynamic properties, and bond dissociation energies of bromomethanes and bromomethyl radicals were published.[19−21]

Table 1 summarizes the available results of the experimental studies of the reaction of OH with CH_2Br_2. The rate constant was measured by absolute techniques by Mellouki et al.[22] and Zhang et al.[23] as well as by relative techniques by DeMore[24] and Orlando et al.[25] It was also measured recently in our laboratory at 298 K.[26] In general, all measurements agree with the value $k(298\ K) = 1.2 \times 10^{-13}$ cm^3 molecule^{-1} s^{-1}.

The kinetic parameters for the reaction of OH with CH_2Br_2 are consistent with a reaction that takes place by hydrogen abstraction. Recent work has demonstrated that the reaction of the hydroxyl radical with CF_3I proceeds rapidly by I atom abstraction.[28] The lack of reactivity of CF_3Br toward OH[27] however argues against any significant contribution of a bromine abstraction reaction pathway for OH + CH_2Br_2.

In this work, the energetics (heat of reactions and reaction barriers) as well reaction rate constants in the temperature range 250−400 K are computed at different levels of theory and basis sets. From the computed temperature dependence data, Arrhenius parameters (*A*-factor and activation energy) are obtained and the results compared to available experimental data.

10.1021/jp991022e
Published on Web 03/14/2000

TABLE 1: Experimental Rate Parameters for the Reaction OH + CH_2Br_2 → H_2O + $CHBr_2$

A (cm^3 molecule^{-1} s^{-1})	E_a (kJ mol^{-1})	T (K)	k(298 K) (cm^3 molecule^{-1} s^{-1})	method	ref
1.9×10^{-12}	7.0	244−370	$1.1_4 \times 10^{-13}$	FP/LIF[a]	22
1.9×10^{-12}	7.0	293−375	1.1×10^{-13}	RR[b]	24
3.2×10^{-12}	7.5	293−375	1.5×10^{-13}	RR[b]	24[e]
		298	1.2×10^{-13}	RR[b]	25
1.5×10^{-12}	6.0	288−368	1.3×10^{-13}	DF/RF[c]	23
		298	1.2×10^{-13}	FP/RF[d]	26

[a] FP/LIF = flash photolysis/laser-induced fluorescence. [b] RR = relative rate. [c] DF/RF = discharge flow/resonance fluorescence. [d] FP/RF = flash photolysis/resonance fluorescence. [e] Rate constants from ref 24 recalculated using the values of the rate constant for the reference reaction OH + CH_2Cl_2 reported in ref 27.

Computational Methods[29]

All calculations described below were carried out with the Gaussian 94[30] suite of programs on a Cray C90/6256 supercomputer and a 32-processor Silicon Graphics Origin 2000 parallel computer. Fully optimized geometries, harmonic vibrational frequencies, and zero-point energy corrections (ZPE) of reactants, the transition structure, and products were calculated with the unrestricted second-order Møller−Plesset perturbation theory (UMP2) using the 6-311G(d,p) and 6-311G(2d,2p) basis sets. Electron correlation was calculated with second- and fourth-order Møller−Plesset perturbation theory in the space of single, double, triple, and quadruple excitations with full annihilation of spin contamination[31] as implemented in the Gaussian 94 package (noted in our results as PMPn, with $n = 2$ or 4). These single-point calculations were carried out using basis sets ranging from 6-311G(2d,2p) to 6-311++G(3df,3pd) and geometries previously optimized at the MP2/6-311G(2d,2p) level. All relative energies quoted and discussed in the present paper include zero-point energy corrections with unscaled vibrational frequencies. For comparison purposes, single-point energies at the MP2/6-311G(2d,2p)-optimized geometries were also computed with the highly correlated (and computationally more expensive) coupled cluster method including single and double electron excitations computed iteratively, and triple excitations computed in a noniteratively manner from the Hartree−Fock determinant, CCSD(T).[32] The larger basis 6-311++G(3df,3pd) was used in these calculations.

Canonical transition-state theory[33] (TST) and tunneling corrections were used to predict the rate constant over the same range of temperatures as the available experimental measurements (250−400 K). Thus, rate constants, $k(T)$, were computed with the following expression:

$$k(T) = \Gamma(T)\frac{k_B T}{\hbar}\frac{Q^{TS}(T)}{Q^{OH}(T)\,Q^{CH_2Br_2}(T)}\exp\left(-\frac{\Delta E}{k_B T}\right) \qquad (1)$$

where: $Q^{TS}(T)$, $Q^{OH}(T)$, and $Q^{CH2Br2}(T)$ are the total partition functions for the transition state, hydroxyl radical, and dibromomethane at temperature T, ΔE is the activation energy including thermal corrections to the internal energy and zero-point energy, k_B is Boltzmann's constant, and $\hbar$ is Planck's constant. $\Gamma(T)$ in eq 1 indicates the corresponding tunneling correction at temperature T (see the Results and Discussion).

Results and Discussion

1. Geometry Parameters and Vibrational Frequencies. *1.1. Geometry Parameters. Reactants and Products.* Table 2 lists the geometry parameters fully optimized at the MP2/6-311G(d,p) and MP2/6-311G(2d,2p) levels of theory. In addition, the available experimental data characterizing the structures of these species are also shown for comparison purposes. As the results show, the optimized geometries with both basis sets are in excellent agreement with the corresponding experimental values.

TABLE 2: Optimized Geometry Parameters[a] for Reactants and Products Involved in H Abstraction Reaction of CH_2Br_2 with Hydroxyl Radicals

		MP2 6-311G(d,p)	MP2 6-311G(2d,2p)	exptl
OH	r(OH)	0.967	0.965	0.971[b]
CH_2Br_2	r(CH)	1.086	1.078	1.097[c]
	r(CBr)	1.929	1.933	1.925
	θ(HCH)	111.6	111.9	110.9
	θ(BrCH)	107.8	107.9	
	ϕ(BrCHH)	118.2	118.5	
H_2O	r(OH)	0.958	0.957	0.958[d]
	θ(HOH)	102.4	103.3	104.5
$CHBr_2$	r(CH)	1.082	1.074	
	r(CBr)	1.860	1.861	
	θ(BrCH)	116.0	116.1	
	ϕ(BrCHBr)	148.4	149.2	

[a] Bond lengths are in angstroms; bond angles θ and dihedral angles ϕ are in degrees. [b] Reference 34. [c] Reference 40. [d] Reference 41.

Transition-State Structure. The MP2-optimized parameters for the transition-state structure using the 6-311G(d,p) and 6-311G(2d,2p) basis sets are shown in Table 3 and Figure 1. Comparison of the results shows that, as in the case of reactants and products, the transition-state structures optimized with both basis sets are very similar. This agreement is further reflected in the transition-state parameter L, defined as the ratio of the increase in the length of the C−H bond being broken and the elongation of the O−H bond being formed, each with respect to its equilibrium value in the reactant (CH_2Br_2) and the product (H_2O).[12] This parameter characterizes the most important aspect of the geometric structure of the transition state. As the results in Table 3 show, addition of an extra set of d-orbital polarization functions on the heavy atoms (C and Br) and two p-orbital polarization functions on the H atoms leads to an L value very close to the one obtained at the MP2/6-311G(d,p) level (0.324 vs 0.314). Both values of the L parameter indicate a reactant-like character for the transition-state structure as expected for an exothermic reaction. The fact that the less computationally demanding MP2/6-311G(d,p) level of theory gives results for the geometry of the minima and transition state in excellent agreement with the ones computed with the larger basis 6-311G(2d,2p) suggests that this level may be sufficient for treating systems similar to the one under study. More cases however must be studied before this level of theory can be recommended. In this work, we choose the MP2/6-311G(2d,2p)-optimized geometries for the single-point energy calculations.

1.2. Vibrational Frequencies. The vibrational frequencies, unscaled zero-point energies, and internal energy corrections at 298 K for reactants, the transition state, and products are given in Tables 4 and 5. For reactants and products, calculated vibrational frequencies at MP2/6-311G(d,p) and MP2/6-311G(2d,2p) are about 7% greater than the experimental values. As

TABLE 3: Optimized Geometry Parameters[a] for the Transition State Involved in H Atom Abstraction Reaction of CH_2Br_2 with Hydroxyl Radicals

	MP2 6-311G(d,p)	MP2 6-311G(2d,2p)	param[a]	MP2 6-311G(d,p)	MP2 6-311G(2d,2p)
$r(C-H_R)$	1.192	1.188	$\theta(Br_{(b)}CH_R)$	108.0	107.8
$r(CH)$	1.087	1.078	$\theta(OH_RC)$	166.2	165.3
$r(CBr_{(a)})$	1.910	1.911	$\theta(HOH_R)$	97.1	97.2
$r(CBr_{(b)})$	1.917	1.919	$\phi(Br_{(a)}CH_RH)$	117.8	118.1
$r(OH_R)$	1.296	1.296	$\phi(Br_{(b)}CH_RH)$	−118.3	−118.4
$r(HO)$	0.968	0.967	$\phi(OH_RCH)$	48.5	51.9
$\theta(HCH_R)$	108.2	108.2	$\phi(HOH_RC)$	50.7	51.5
$\theta(Br_{(a)}CH_R)$	105.8	106.0	L[b]	0.314	0.324

[a] Bond lengths are in angstroms; bond angles θ and dihedral angles ϕ are in degrees. The hydrogen atom involved in H atom abstraction is noted H_R. (a) refers to the in-plane bromine and (b) to the out-of-plane bromine. [b] The parameter L is the ratio between the elongation value of the C−H bond and the elongation of the O−H bond: $L = \delta r(CH)/\delta r(OH)$.

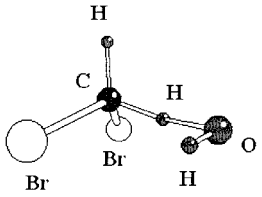

Figure 1. MP2/6-311G(2d,2p)-optimized geometry for the transition state involved in the OH + CH_2Br_2 reaction.

TABLE 4: Calculated[a,b] Vibrational Frequencies (cm^{-1}) for the Reactants, Transition State, and Products Involved in H Atom Abstraction Reaction of CH_2Br_2 with Hydroxyl Radicals

species	vibrational frequencies (cm^{-1})[c]
OH	(*a*) 3853
	(*b*) 3833
	3735[d]
CH_2Br_2	(*a*) 178, 604, 692, 835, 1150, 1265, 1459, 3169, 3254
	(*b*) 175, 590, 672, 833, 1141, 1239, 1458, 3183, 3270
	169, 588, 653, 812, 1095, 1195, 1382, 3009, 3073[e]
TS	(*a*) 2075i, 70, 102, 155, 183, 473, 651, 713, 805, 959, 1210, 1319, 1405, 3211, 3840
	(*b*) 2200i, 76, 109, 156, 182, 463, 640, 698, 803, 957, 1191, 1307, 1395, 3225, 3811
H_2O	(*a*) 1667, 3905, 4013
	(*b*) 1685, 3875, 3989
	1595, 3657, 3756[e]
$CHBr_2$	(*a*) 193, 492, 653, 805, 1241, 3267
	(*b*) 189, 486, 644, 790, 1214, 3279
	633, 778, 1164[f]

[a] MP2/6-311G(d,p). [b] MP2/6-311G(2d,2p). [c] The experimental values of the vibrational frequencies are in italics. [d] Reference 34. [e] Reference 42. [f] Reference 43.

TABLE 5: Calculated Zero-point Energy and Thermal Energy Corrections at 298 K for the Reactants, Transition State, and Products Involved in H Atom Abstraction Reaction of CH_2Br_2 with Hydroxyl Radicals

	zero-point Energy[a]	thermal energy[a]		zero-point energy[a]	thermal energy[a]
OH	23.1[b]/ 22.9[c]	6.2	$CHBr_2$	39.8/39.5	10.2
CH_2Br_2	75.4/75.1	10.1	TS	90.3/89.8	16.4
H_2O	57.3/57.1	7.5			

[a] Units are kJ mol^{-1}. [b] Geometry optimization calculation at the MP2/6-311G(d,p) level of theory. [c] Geometry optimization calculation at the MP2/6-311G(2d,2p) level of theory.

with the geometries, the vibrational frequencies computed with both basis sets are in excellent agreement. The eigenvector in the transition state corresponding to the imaginary frequency is primarily a motion of the reactive hydrogen atom being transferred between the C and the O centers. The calculated imaginary frequency is about 6% larger at the MP2/6-311G(2d,2p) level of theory than at the MP2/6-311G(d,p) level (2200 cm^{-1} vs 2075 cm^{-1}). A similar fact was observed previously in the series of H atom abstraction reactions F + $CHCl_{3-x}F_x$ (x = 0, 1, 2, or 3).[13]

2. Reaction Enthalpies and Activation Energies. Table 6 lists reaction enthalpies (Δ_rH), C−H bond strengths $D_{298}(H-CHBr_2)$, and activation energies (E_a), computed at different levels of theory and taking into account the zero-point energy differences and thermal energy corrections at 298 K (calculated using the vibrational frequencies given in Table 4) for the reaction OH + CH_2Br_2. Results obtained at the highly correlated level CCSD(T)/6-311++G(3df,3pd)//MP2/6-311G(2d,2p) are also listed for comparison purposes.

2.1. Reaction Enthalpies. Reaction enthalpies calculated at the PMP2/6-311G(d,p)//MP2/6-311G(d,p) and PMP2/6-311G(2d,2p)//MP2/6-311G(2d,2p) levels are very close to the literature values based on $\Delta_fH°$ at 298 K for OH,[34] CH_2Br_2,[39] H_2O,[34] and $CHBr_2$,[40] especially if the experimental uncertainties for CH_2Br_2 (±9 kJ mol^{-1}) and $CHBr_2$ (±5 kJ mol^{-1}) are taken into consideration. Adding diffuse functions to the basis sets at the PMP2 level leads to reaction enthalpies significantly larger than the experimental value and outside the experimental uncertainties. A better agreement with experiment is obtained at the PMP4(SDTQ) level.

To improve on the agreement between *ab initio* and experimental values, especially in the case where basis sets have been expanded by including diffuse functions, reaction enthalpies for reaction R1 were also corrected by new values of $D_{298}(H-CHBr_2)$ computed at different levels of theory using the following isodesmic reaction:

$$CH_3 + CH_2Br_2 \rightarrow CH_4 + CHBr_2 \qquad (R2)$$

The direct calculation of this bond dissociation energy from the reaction $CH_2Br_2 \rightarrow H + CHBr_2$ is expected to be systematically in error due to insufficient treatment of electron correlation and incompleteness of the basis sets. The use of an isodesmic reaction, such as reaction R2, provides an indirect method that may lead to a more reliable value of the bond dissociation energy. In general, isodesmic reactions are characterized by having the same number and types of bonds on each side of the equation, so that the errors mentioned above are largely canceled when $D_{298}(H-CHBr_2)$ is calculated. The reaction enthalpy for reaction R2 was computed at the same levels of theory as that for reaction R1. Taking the experimental value of $D_{298}(H-CH_3)$ = 440 kJ mol^{-1},[41] we obtain calculated $D_{298}(H-CHBr_2)$ values at the various levels of theory used in this work (Table 6, column 3). These $D_{298}(H-CHBr_2)$ quantities were then used in the calculation of the reaction enthalpy for reaction R1 by means of the following relation:

$$\Delta_rH(ISO) = D_{298}(H-CHBr_2) - D_{298}(H-OH) \qquad (2)$$

TABLE 6: Reaction Enthalpies $\Delta_r H$, Bond Strengths $D_{298}(H-CHBr_2)$, Reaction Enthalpies $\Delta_r H$ (ISO) Calculated Using an Isodesmic Reaction, and Activation Energies E_a Calculated at 298 K for the Reaction $OH + CH_2Br_2 \rightarrow H_2O + CHBr_2$ at Various Levels of Theory

level of theory[a]	$\Delta_r H^{b,d}$	$D_{298}(H-CHBr_2)^d$	$\Delta_r H(ISO)^{b,d}$	$E_a^{c,d}$
PMP2/6-311G(d,p)	−82.7	412.7	−86.1	20.3
PMP2/6-311G(2d,2p)	−86.0	415.1	−83.7	17.4
PMP2/6-311G(2df,2p)	−91.1	412.1	−86.7	13.9
PMP2/6-311G(3df,2p)	−92.4	411.3	−87.5	12.0
PMP4(SDTQ)/6-311G(3df,2p)	−79.1	409.3	−89.5	13.0
PMP2/6-311++G(3df,2p)	−100.4	413.3	−85.5	14.6
PMP4(SDTQ)/6-311++G(3df,2p)	−86.4	411.3	−87.5	15.1
PMP2/6-311++G(3df,3pd)	−102.3	414.9	−83.9	10.6
PMP4(SDTQ)/6-311++G(3df,3pd)	−88.7	413.1	−85.7	10.5
CCSD(T)/6-311++G(3df,3pd)	−86.9	410.3	−87.6	7.0
experimental	−81.6[e]	417.1[e]	−81.6[e]	7.0[f]

[a] All the geometry optimization calculations were done with the MP2/6-311G(2d,2p) except the first with MP2/6-311G(d,p). [b] Including the sum of thermal energies (ΔZPE + thermal energy corrections). [c] Including the sum of thermal energies (ΔZPE + thermal energy corrections + RT).[d] In kJ mol^{-1}. [e] See the text. [f] From ref 22.

Table 6 (column 4) lists the $\Delta_r H$(ISO) values obtained by eq 2, which can be compared to the direct calculations (column 2) and to their experimental counterparts. The degree of improvement observed becomes more significant for basis sets with diffuse functions.

2.2. Activation Energies. The results reported in Table 6 indicate that PMP2/6-311G(d,p)//MP2/6-311G(d,p) calculations overestimate the experimental activation energy by about 13−14 kJ mol^{-1}. Adding an extra set of d and p functions to the basis sets decreases the activation energy by about 3.0 kJ mol^{-1}. Addition of more polarization and diffuse functions tends to improve the agreement with experiment. Thus, PMP4(SDTQ)/6-311++(3df,3pd) and PMP2/6-311++(3df,3pd) calculations lead to activation energies for the $OH + CH_2Br_2$ reaction that are 3.5 and 3.6 kJ mol^{-1} higher than the experimental value, respectively. Similar calculations using the same basis sets with the highly correlated and more computationally demanding CCSD(T) level of theory predict an activation energy of 7.0 kJ mol^{-1}, in excellent agreement with the experimental value. This result clearly indicates that most of the error in the activation energies computed at PMP2 and PMP4 with the 6-311++G-(3df,3pd) basis can be attributed to the lack of correlation in such methods and not to an improper optimized geometry at the MP2/6-311G(2d,2p) level of theory. It is interesting to note that, at the PMP2 and PMP4 levels, a better agreement with experiment is achieved when the 6-311G(3df,2p) basis is used when compared to the larger 6-311++G(3df,2p) basis. This result is most probably a reflection of a better balance between basis set size and correlation in the case of the smaller basis. Similar results have been observed by Truong and Truhlar[44] in their *ab initio* transition-state theory calculations of the reaction rate for $OH + CH_4 \rightarrow H_2O + CH_3$.

The objective of the present work is to develop a method that can be applied to a range of reactants, typically much larger than CH_2Br_2. Thus, although the CCSD(T) level of theory results in better values of the activation energy, it is too computationally intensive to be generally applicable at the present time. Therefore, in this work, we have chosen the energetics computed at PMP4(SDTQ)/6-311++G(3df,3pd)//MP2/6-311G(2d,2p) to calculate the reaction rate constants (see below). These rate constants are determined as a function of temperature and an activation energy calculated from this dependence.

3. Kinetic Parameters and Tunneling Effect. The calculation of the reaction rate constants using the TST formula given in eq 1 requires the proper computation of the partition functions of reactants and the transition state. In general, the total partition function $Q^X(T)$ of species X (X = CH_2Br_2, OH, or TS) can be cast in terms of the translational ($Q^X{}_T$), rotational ($Q^X{}_R$), electronic ($Q^X{}_e$), and vibrational ($Q^X{}_v$), partition functions:

$$Q^X(T) = Q^X{}_T(T)\, Q^X{}_R(T)\, Q^X{}_e(T)\, Q^X{}_v(T) \qquad (3)$$

In computing the electronic partition function for the OH radical, $Q^{OH}{}_e$, the multiplicity of the states $^2\Pi_{3/2}$ and $^2\Pi_{1/2}$ and the energy gap of 139.7 cm^{-1} between the levels[34] have been taken into consideration.

3.1. Hindered Rotor Approximation. Direct inspection of the TS low-frequency modes (Table 4) indicates that the mode with a frequency of 109 cm^{-1} consists of a hindered OH rotation about the nearly linear C−H−O axis with a rotational barrier of 5.5 kJ mol^{-1}. Consequently, this mode should be treated as a hindered rotor instead of a vibration.[43] Thus, this mode was removed from the vibrational partition function for the TS, and the corresponding hindered rotor partition function $Q_{HR}(T)$ was calculated, yielding the following expression for the total TS partition function:

$$Q^{TS} = Q^{TS}{}_T(T)\, Q^{TS}{}_R(T)\, Q^{TS}{}_e(T)\, Q^{TS}{}_{v'}(T)\, Q_{HR}(T) \qquad (4)$$

with $Q^{TS}{}_{v'}(T)$ being the corrected vibrational partition function where the internal rotation mode has been removed.

In our calculations we have adopted the analytical approximation to $Q_{HR}(T)$ for a one-dimensional hindered internal rotation proposed by Ayala and Schlegel:[44]

$$Q_{HR}(T) = \left(\frac{Q_i^{h.o.q}}{Q_i^{h.o.cl}}\right) Q_i^{FR} \frac{\left(1 + P_2 \exp\left[-\frac{V_0}{2k_BT}\right]\right)}{\left(1 + P_1 \exp\left[-\frac{V_0}{2k_BT}\right]\right)} \exp\left[-\frac{V_0}{2k_BT}\right] J_0\left(\frac{iV_0}{2k_BT}\right) \qquad (5)$$

where T is the temperature, k_B is Boltzmann's constant, V_0 is the internal rotational barrier, Q_i^{FR} is the free-rotor partition function, P_1 and P_2 are polynomial functions of $1/Q_i^{FR}$ and V_0/kT, J_0 is Bessel's function, and $Q_i^{h.o.q}$ and $Q_i^{h.o.cl}$ are the quantum and classical partition functions defined as

$$Q_i^{h.o.q} = \frac{e^{-u/2}}{1 - e^{-u}} \quad \text{and} \quad Q_i^{h.o.cl} = \frac{1}{u}, \quad u = \frac{\hbar \nu_i}{k_B T} \qquad (6)$$

with ν_i being the vibrational frequency associated with the hindered rotation (109 cm^{-1}). Again following Ayala's and

Schlegel's recommendation,[44] we have used the following approximation for the free-rotor partition function:

$$Q_i^{FR}(T) = \left(\frac{8\pi^3 k_B}{\hbar^2 \sigma^2}\right)^{1/2} (I_R T)^{1/2} \qquad (7)$$

where I_R is the reduced moment of inertia for the internal rotation, σ is the periodicity of the internal rotation potential, and the rest of the symbols have the same meaning as in the previous equations. For the case of the $OH + CH_2Br_2$ transition-state structure, $\sigma = 1$, $V_0 = 5.5$ kJ mol^{-1}, and $I_R = 1.52 \times 10^{-47}$ kg m^2 calculated at MP2/6-311G(2d,2p) were used to compute the free-rotor partition functions by means of eq 7.

3.2. Tunneling. Reactions involving hydrogen atom transfers are usually characterized by significant tunneling effects that must be accounted for when computing reaction rate constants. Tunneling is the result of quantum effects that couple the reaction path coordinate to the other degrees of freedom of the reacting system due to the curvature along the reaction path. In these cases, the separation of the reaction coordinate from the other degrees of freedom is no longer valid and tunneling can occur through a variety of paths involving all coordinates. Given that the quantum mechanical treatment of tunneling in a multidimensional potential energy surface is very complicated, the TST reaction rate constant is computed assuming the separability of the reaction path and further corrected by a tunneling correction factor $\Gamma(T)$ (see eq 1). In the present work, three expressions for tunneling corrections have been explored. The first consists of a closed form approximation for $\Gamma(T)$ obtained by Wigner[45] in 1932 using a method which is, to a first approximation, applicable to any shape of potential curve:

$$\Gamma(T) = 1 + \frac{1}{24}\left(\frac{\hbar \nu^{\ddagger}}{k_B T}\right)^2 \qquad (8)$$

where $\nu^{\ddagger}$ is the imaginary frequency at the saddle point. In the second method, $\Gamma(T)$ is computed with the one-dimensional unsymmetrical potential developed by Eckart:[33a,46]

$$V(s) = \frac{Ay}{(1+y)} + \frac{By}{(1+y)^2}; \quad y = \exp\left(\frac{2\pi s}{L}\right) \qquad (9)$$

where s is the reaction coordinate, L is the barrier width, and the parameters A and B depend on the forward and reverse energy barriers, ΔV_1 and ΔV_2. The parameters A, B, and L in eq 9 are related to ΔV_1 and ΔV_2 by

$$A = \Delta V_2 - \Delta V_1$$

$$B = [\Delta V_1^{1/2} + \Delta V_2^{1/2}]^2$$

$$L = 2\pi\left(-\frac{2}{F^*}\right)^{1/2}\left[\frac{1}{\Delta V_1^{1/2}} + \frac{1}{\Delta V_2^{1/2}}\right]^{-1} \qquad (10)$$

with F^* equal to the force constant evaluated at the maximum of the potential. The third method is based on the symmetrical Eckart potential, which is obtained by making parameter A in eq 9 and 10 equal to zero. In this case, the following closed form for the tunneling correction is obtained:

$$\Gamma(T) = 1 + \frac{1}{24}\left(\frac{\hbar \nu^{\ddagger}}{k_B T}\right)^2 \left(1 + \frac{k_B T}{\Delta V_1}\right) \qquad (11)$$

These three different expressions were then employed in two different approaches to the calculation of $\Gamma(T)$. In the first approach, the unsymmetrical Eckart potential given by eqs 9 and 10 was fitted using the forward (ΔV_1) and reverse (ΔV_2) barriers obtained at the MP2/6-311G(2d,2p) level of theory, as well as the imaginary frequency computed at the same level of theory ($\nu^{\ddagger} \approx 2200$ cm^{-1}). The resulting potential was finally used to compute $\Gamma(T)$ by numerical integration of the analytical Eckart transmission probability[46] using an efficient algorithm developed by Brown.[47] Wigner and symmetrical Eckart tunneling corrections were computed by eqs 8 and 11, respectively, using the MP2/6-311G(2d,2p) imaginary frequency.

In the second approach, the reaction path computed at the MP2/6-311G(2d,2p) level using Gonzalez and Schlegel's second-order IRC algorithm[48] with a step size of 0.05 bohr amu$^{1/2}$ was fit to the following Eckart function:

$$V(s) = \sum_{i=1}^{3}\left[\frac{A_i y_i}{(1+y_i)} + \frac{B_i y_i}{(1+y_i)^2}\right] \qquad (12)$$

where $y_i = \exp[c_i(s - s_0)]$ and A_i, B_i, c_i, and s_0 are constants. In the fitting procedure, an RMS of 4×10^{-2} kJ mol^{-1} was obtained. The fitted parameters together with eq 12 were then used to interpolate the necessary IRC points to fit the Eckart potential given by eqs 9 and 10 in the vicinity of the transition state (-0.3 bohr amu$^{1/2} \le s \le +0.3$ bohr amu$^{1/2}$) with the constraint that the difference between the forward and reverse barriers is equal to the heat of reaction computed at the MP2/6-311G(2d,2p) level ($\Delta V_1 - \Delta V_2 = \Delta H_{rxn} = -82.68$ kJ mol^{-1}). In this step, the imaginary frequency was not fixed to the MP2 value, and it was considered as another fitting parameter. This procedure gave an r^2 approximately equal to 0.97 and a standard deviation of 0.30. An imaginary frequency significantly lower than the one obtained at the MP2/6-311G(2d,2p) level was found (1245 cm^{-1} vs 2200 cm^{-1}). The parameters generated by this second fitting were used together with the Eckart potential (eqs 9 and 10) to compute the corresponding unsymmetrical Eckart tunneling correction using the same integration scheme described in the previous approach. In addition, the imaginary frequency obtained from this fitting (1245 cm^{-1}) was used to compute the Wigner (eq 8) and symmetrical Eckart (eq 11) tunneling corrections. In this work we refer to the Wigner, symmetrical and unsymmetrical Eckart tunneling corrections computed by these two approaches as W-I, SE-I, UE-I, W-II, SE-II, and UE-II, respectively. In both UE-I and UE-II the fitting of eqs 9 and 10 was carried out with the constraint that the heat of reaction was given by the difference between the forward and reverse barriers ($\Delta H_{rxn} = \Delta V_1 - \Delta V_2$). The significantly small value of the imaginary frequency obtained by the UE-II method when compared to the value obtained at the MP2 level indicates that UE-I tunneling corrections are expected to be larger than the corresponding UE-II values.

It is important to note that the tunneling corrections obtained by either Wigner's formalism or the symmetrical and unsymmetrical Eckart potentials are just approximations based on a one-dimensional representation of the surface and, as in the case of the Eckart potentials, on an *a priori* assumption of the shape of the barrier. More sophisticated and computationally demanding algorithms such as the ones developed by Truhlar[49] and Miller[50] should be used if more accurate results are necessary. In these methods, detailed knowledge of the reaction path is needed, making the computation of tunneling corrections of relatively large electronic structure systems such as the ones containing bromine atoms very time-consuming. Given that the purpose of the proposed screening tools (see the Introduction) is to develop a set of inexpensive methodologies leading to a

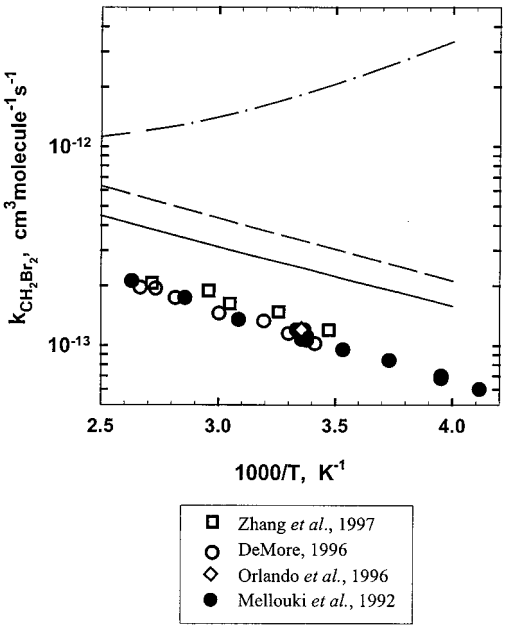

Figure 2. Temperature dependence of the rate constants for the reaction of CH_2Br_2 with OH computed at PMP4(SDTQ)/6-311++G(3df,3pd)//MP2/6-311G(2d,2p) using the imaginary frequency computed at the MP2/6-311G(2d,2p) level. Solid line: Wigner tunneling correction W-I. Short dashed line: symmetrical Eckart tunneling correction SE-I. Dashed−dotted line: unsymmetrical Eckart tunneling correction UE-I. UE-I tunneling correction was computed after fitting expression 9 to the forward and reverse barrier, using the MP2/6-311G(2d,2p) imaginary frequency.

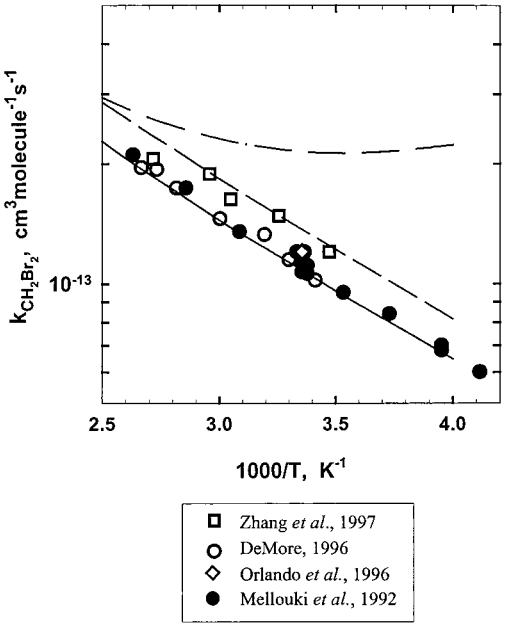

Figure 3. Temperature dependence of the rate constants for the reaction of CH_2Br_2 with OH computed at PMP4(SDTQ)/6-311++G(3df,3pd)//MP2/6-311G(2d,2p). Solid line: Wigner tunneling correction W-II. Short dashed line: symmetrical Eckart tunneling correction SE-II. Dashed−dotted line: unsymmetrical Eckart tunneling correction UE-II. In all cases, the imaginary frequency was obtained by the fitting of the Eckart function 8 to the results of the MP2/6-311G(2d,2p) IRC as described in the text.

semiquantitative description of the kinetics of hydrogen abstraction reactions of haloalkanes by OH radicals, the use of approximated methods such as Wigner and Eckart tunneling corrections are adequate for the purpose of this work.

The results of the calculations of the rate constants at the PMP4/6-311++G(3d,3pd)//MP2/6-311G(2d,2p) level of theory using tunneling corrections previously discussed are shown in Figures 2 and 3. As Figure 2 shows, the rate constants computed with the unsymmetrical Eckart tunneling correction UE-I are significantly larger than the experimental values. In addition, it is observed that UE-I predicts the wrong shape of the Arrhenius plot. Similar results have been reported[51] in the case of reactions between OH and CHF_3, CH_2F_2, CH_3F, CHF_3, and CH_4. Wigner and symmetrical Eckart tunneling corrections computed by methods W-I and SE-I predict reaction rate constants that are consistently larger than the experimental values over the whole temperature range. These methods, however, reproduce the shape of the experimental curve, contrary to the unsymmetrical Eckart potential. In addition, the theoretical results computed with W-I are in better agreement with the experimental rate constants than the results obtained with symmetrical Eckart tunneling, SE-I.

In all of the calculations with approach II, a better agreement with the experimental values is observed than with approach I, in particular in the case of W-II, where the predicted rate constants are in excellent agreement with the experimental values over the whole temperature range. Despite the better behavior in the temperature range 380−400 K, the unsymmetrical Eckart method UE-II still overestimates the rate constants, producing a curved Arrhenius plot unlike the experimental data (see Figure 3). As in the previous case, symmetrical Eckart and Wigner corrections SE-II and W-II reproduce the shape of the experimental curve. The failure of unsymmetrical Eckart to reproduce the right shape of the Arrhenius plot can probably be attributed to the prediction of a too thin and sharp potential barrier, which results in the overestimation of tunneling, especially at low temperatures. This is not surprising given that the shape of the barrier predicted by unsymmetrical Eckart is more representative of large tunneling processes such as heavy−light−heavy abstractions. These conclusions seem to be supported by the fact that Wigner and symmetrical Eckart tunneling corrections predict the right shape of the Arrhenius plot. It is well known that these tunneling corrections work well in cases where the potential barriers are broad and tunneling is not so large. In addition, the improvement observed in the results of UE-II relative to UE-I is an indication of how the fit of the unsymmetrical Eckart potential to the IRC in the vicinity of the transition state provides a better description of the shape of the potential at the top of the barrier. An in-depth study of the applicability and limitations of unsymmetrical Eckart tunneling corrections in hydrogen abstractions is beyond the goal of this work. A more systematic study of this and related issues concerning tunneling will be addressed in a future publication.

The Arrhenius expression $k(T) = A \exp(-E_a/RT)$ fitted to the rate constants computed with the Wigner tunneling correction in the temperature range 250−400 K gives the Arrhenius parameters $A = 2.5 \times 10^{-12}$ cm^{-3} molecule^{-1} s^{-1} and $E_a/R =$ 690 K computed with the W-I method and $A = 1.8 \times 10^{-12}$ cm^{-3} molecule^{-1} s^{-1} and $E_a/R = 835$ K computed with the more expensive method W-II. Both results are in good agreement with the experimental values[27] $A = 2.4 \times 10^{-12}$ cm^{-3} molecule^{-1} s^{-1} and $E_a/R = 900$ K and result in rate constants within a factor of 2 of the experimental values over the range of atmospheric interest. Since the W-I method does not require a detailed knowledge of the reaction path, it is concluded that it may be the method of choice for the screening tool proposed in this work. Table 7 lists the reaction rate constants computed at 250, 298, and 400 K using the Arrhenius expression obtained with

TABLE 7: Summary of Rate Constants ($cm^3 \cdot molecule^{-1} \cdot s^{-1}$) Calculated at PMP4(SDTQ)/6-311++G(3df,3pd)//UMP2/6-311G(2d,2p) Including the Wigner Tunneling Correction

	250 K	298 K	400 K
k(theory, this work)[a]	1.6×10^{-13}	2.5×10^{-13}	4.5×10^{-13}
k(experimental, JPL 1997)	0.7×10^{-13}	1.2×10^{-13}	2.5×10^{-13}
k(theory)/k(experimental)	2.3	2.1	1.8

[a] Computed using the following Arrhenius expression: $k(T) = 2.5 \times 10^{-12} \exp(-690/T)$ fitted to the theoretical results obtained in this work in the temperature range 250−400 K.

the W-I method as well as the corresponding experimental values.

The results shown in Figures 2 and 3 as well as Table 7 seem to indicate that at least in the temperature range under study (250−400 K), rate constants computed at the PMP4/6-311++G(3d,3pd)//MP2/6-311G(2d,2p) level using Wigner tunneling corrections provide a viable methodology for the implementation of the proposed screening tool in the case of hydrogen abstractions from haloalkanes by OH radicals. Preliminary studies[52] on several different hydrogen abstraction reactions involving OH and a series of halogenated substituted methanes $CX_nY_mH_{4-n-m}$ (X = Cl, F, Br) support this conclusion. More cases should be included in this systematic study however before a final recommendation can be made.

Conclusion

Ab initio calculations were performed at different levels of theory for the H atom abstraction reaction between dibromomethane and the hydroxyl radical. The geometry parameters for the reactants, products, and transition state were fully optimized at the MP2 level of theory with the 6-311G(d,p) and 6-311G(2d,2p) basis sets. The transition structure parameter L, defined as the ratio between the increase in length of the C−H bond being broken and the elongation of the O−H bond being formed, changes only slightly with the basis sets. The calculation of the energetics of the reaction proved to be more dependent on the level of theory, and on the nature and extent of the basis set. A reaction barrier of 7.0 kJ mol^{-1} is obtained at the highly correlated level CCSD(T)/6-311++G(3df,3pd)//MP2/6-311G(2d,2p), in excellent agreement with the experimental value. Among the lower levels of theory explored in this study, the best agreement with these values was obtained at the PMP4(SDTQ)/6-311++G(3df,3pd)//MP2/6-311G(2d,2p) level. The calculation of reaction rate constants over the temperature range 250−400 K using Wigner tunneling corrections reproduces the shape of the experimental Arrhenius plot. It is found that the use of the unsymmetrical Eckart potential in the calculation of tunneling corrections gives reaction rate constants significantly higher than the experimental values. In addition, the predicted Arrhenius plot has the wrong shape. Even though tunneling corrections computed using the symmetrical Eckart potential leads to an Arrhenius plot with the right shape, it consistently predicts rate constants in poorer agreement with experiment than the ones obtained with the Wigner tunneling corrections. These results seem to suggest that PMP4(SDTQ)/6-311++G(3df,3pd)//MP2/6-311G(2d,2p) calculations combined with Wigner tunneling corrections might be a viable methodology for the semiquantitative study of hydrogen abstraction reactions of other haloalkanes by OH radicals. It is important to note that the reasonable success of the Wigner tunneling corrections in these types of reactions should not be used to generalize the superiority of this method over more sophisticated techniques. Rather, these results should be critically analyzed in the context of the creation of a very computationally inexpensive screening tool that will allow the prediction of the atmosphere lifetimes of new chemical species.

Acknowledgment. This work was supported by the Upper Atmosphere Research Program of the National Aeronautics and Space Administration and by the Next Generation Fire Suppression Technology Program, funded by the Department of Defense Strategic Environmental Research and Development Program under MIPR Number W74RDV73243630. We are grateful to D. Burgess, V. Orkin, and Tom Allison (NIST) for helpful discussions, and to the anonymous reviewers for their useful comments.

References and Notes

(1) Noto, T.; Babushok, V.; Burgess, D. R.; Hamins, A.; Tsang, W.; Miziolek, A. *Twenty-Sixth Symp. (Int.) Comb.* **1996**, 1377.
(2) Jeong, K. M.; Kaufman, F. *J. Phys. Chem.* **1982**, *86*, 1816.
(3) Cohen, N.; Benson, S. W. *J. Phys. Chem.* **1987**, *91*, 162.
(4) Bottoni, A.; Poggi, G.; Emmi, S. S. *J. Mol. Struct.: THEOCHEM* **1993**, *279*, 299.
(5) Fu, Y.; Lewis-Bevan, W.; Tyrell, J. *J. Phys. Chem.* **1995**, *99*, 630.
(6) Schwartz, M.; Marshall, P.; Berry, R. J.; Ehlers, C. J.; Petersson, G. A. *J. Phys. Chem. A* **1998**, *102*, 10074.
(7) Martell, J. M.; Boyd, R. J. *J. Phys. Chem.* **1995**, *99*, 13402.
(8) Sekusak, S.; Gusten, H.; Sabljic, A. *J. Chem. Phys.* **1995**, *102*, 7504.
(9) Sekusak, S.; Gusten, H.; Sabljic, A. *J. Phys. Chem.* **1996**, *100*, 6212.
(10) Sekusak, S.; Sabljic, A. *Chem. Phys. Lett.* **1997**, *272*, 353.
(11) Sekusak, S.; Liedl, K. R.; Rode, B. M.; Sabljic, A. *J. Phys. Chem. A* **1997**, *101*, 4245.
(12) Rayez, M.-T.; Rayez, J.-C.; Sawerysyn, J.-P. *J. Phys. Chem.* **1994**, *98*, 11342.
(13) Louis, F. Ph.D. Thesis University of Lille: Lille, France, 1997.
(14) Louis, F.; Rayez, M.-T.; Rayez, J.-C.; Sawerysyn, J.-P. *Phys. Chem. Chem. Phys.* **1999**, *3*, 383.
(15) Talhaoui, A.; Louis, F.; Devolder, P.; Meriaux, B.; Sawerysyn, J.-P.; Rayez, M.-T.; Rayez, J.-C. *J. Phys. Chem.* **1996**, *100*, 13531.
(16) Louis, F.; Talhaoui, A.; Sawerysyn, J.-P.; Rayez, M.-T.; Rayez, J.-C. *J. Phys. Chem. A* **1997**, *101*, 8503.
(17) Bernardi, F.; Bottoni, A. *J. Phys. Chem. A* **1997**, *101*, 1912.
(18) Berry, R. J.; Burgess, D. R. F.; Nyden, M. R.; Zachariah, M. R. *J. Phys. Chem.* **1995**, *99*, 17145.
(19) Paddison, S. J.; Tschuikow-Roux, E. *J. Phys. Chem.* **1998**, *102*, 6191.
(20) Paddison, S. J.; Tschuikow-Roux, E. *Int. J. Thermophys.* **1998**, *19*, 719.
(21) Kambanis, K. G.; Lazarou, Y. G.; Papagiannakopoulos, P. *J. Phys. Chem. A* **1997**, *101*, 8496.
(22) Mellouki, A.; Talukdar, R. K.; Schmoltner, A. M.; Gierczak, T.; Mills, M. J.; Solomon, S.; Ravishankara, A. R. *Geophys. Res. Lett* **1992**, *19*, 2059.
(23) Zhang, D. Q.; Zhong, J. X.; Qiu, L. X. *J. Atmos. Chem.* **1997**, *27*, 209.
(24) DeMore, W. B. *J. Phys. Chem.* **1996**, *100*, 5813.
(25) Orlando, J. J.; Tyndall, G. S.; Wallington, T. J.; Dill, M. *Int. J. Chem. Kinet.* **1996**, *28*, 433.
(26) Orkin, V.; Huie, R. E.; Kurylo, M. J. Unpublished work.
(27) DeMore, W. B.; Sander, S. P.; Golden, D. M.; Hampson, R. F.; Kurylo, M. J.; Howard, C. J.; Ravishankara, A. R.; Kolb, C. E.; Molina, M. J. *JPL Publication 97-4*; 1997, *Evaluation 12*.
(28) Berry, R. J.; Yuan, J.; Misra, A.; Marshall, P. *J. Phys. Chem. A* **1998**, *102*, 5182.
(29) The identification of commercial equipment or materials does not imply recognition or endorsement by the National Institute of Standards and Technology, nor does it imply that the material or equipment identified are necessarily the best available for the purpose.
(30) Frisch, M. J.; Trucks, G. W.; Schlegel, H. B.; Gill, P. M. W.; Johnson, B. G.; Robb, M. A.; Cheeseman, J. R.; Keith, T.; Petersson, G. A.; Montgomery, J. A.; Raghavachari, K.; Al-Laham, M. A.; Zakrzewski, V. G.; Ortiz, J. V.; Foresman, J. B.; Cioslowski, J.; Stefanov, B. B.; Nanayakkara, A.; M. Challacombe; Peng, C. Y.; Ayala, P. Y.; Chen, W.; Wong, M. W.; Andres, J. L.; Replogle, E. S.; Gomperts, R.; Martin, R. L.; Fox, D. J.; Binkley, J. S.; Defrees, D. J.; Baker, J.; Stewart, J. P.; Head-Gordon, M.; Gonzalez, C.; Pople, J. A. *GAUSSIAN 94*, Revision D.4 ed.; Gaussian, Inc: Pittsburgh, PA, 1995.
(31) (a) Schlegel, H. B. *J. Chem. Phys.* **1986**, *84*, 4530. (b) Schlegel, H. B. *J. Phys. Chem.* **1988**, *92*, 3075. (c) Sosa, C.; Schlegel, H. B. *Int. J. Quantum Chem.* **1986**, *29*, 1001. (d) Sosa, C.; Schlegel, H. B. *Int. J. Quantum Chem.* **1987**, *30*, 155.

(32) (a) Bartlett, R. J.; Purvis, G. D. *Int. J. Quantum Chem.* **1978**, *14*, 516. (b) Cizek, J. *Adv. Chem. Phys.* **1969**, *14*, 35. (c) Purvis, G. D.; Bartlett, R. J. *J. Phys. Chem.* **1982**, *76*, 1910. (d) Scuseira, G. E.; Janssen, C. L.; Schaefer, H. F., III. *J. Chem. Phys.* **1988**, *89*, 7382. (e) Scuseira, G. E.; Schaefer, H. F., III. *J. Chem. Phys.* **1989**, *90*, 3700. (f) Pople, J. A.; Head-Gordon, M.; Raghavachari, K. *J. Chem. Phys.* **1987**, *87*, 5968.

(33) (a) Johnston, H. S. *Gas-Phase Reaction Rate Theory*; The Roland Press Company: New York, 1966. (b) Laidler, K. J. *Theories of Chemical Reaction Rates*; McGraw-Hill: New York, 1969. (c) Weston, R. E.; Schwartz, H. A. *Chemical Kinetics*; Prentice Hall: New York, 1972. (d) Rapp, D. *Statistical Mechanics*; Holt, Reinhard, and Winston: New York, 1972. (e) Nikitin, E. E. *Theory of Elementary Atomic and Molecular Processes in Gases*; Claredon Press: Oxford, 1974. (f) Smith, I. W. M. *Kinetics and Dynamics of Elementary Gas Reactions*; Butterworth: London, 1980. (g) Steinfield, J. I.; Francisco, J. S.; Hase, W. L. *Chemical Kinetics and Dynamics*; Prentice Hall: Englewood Cliffs, New Jersey, 1989. (h) Rate constants calculated with the Turbo-Rate module in the β version of the TURBO−OPT geometry optimization package, developed by C. Gonzalez, National Institute of Standards and Technology, Gaithersburg, MD.

(34) Chase, M. W. *J. Phys. Chem. Ref. Data* **1998**, *Monograph 9*.

(35) Bickerton, J.; Minas da Piedade, M. E.; Pilcher, G. *J. Chem. Thermodyn.* **1984**, *16*, 661.

(36) Tschuikow-Roux, E.; Paddison, S. *Int. J. Chem. Kinet.* **1987**, *19*, 15.

(37) Tsang, W. In *Heats of formation of organic free radicals by kinetic methods*; Tsang, W., Ed.; Blackie Academic & Professional: London, 1996; p 22.

(38) Wigner, E. P. *Z. Phys. Chem.* **1932**, *B19*, 203.

(39) Skodje, R. T.; Truhlar, D. G.; Garet, B. C. *J. Chem. Phys.* **1982**, *77*, 5955.

(40) Kudchadker, S. A.; Kudchadker, A. P. *J. Phys. Chem. Ref. Data* **1975**, *4*, 457.

(41) Lide, D. R. In *Handbook of Chemistry and Physics*; Lide, D. R., Ed.; CRC Press: Boca raton, FL, 1990.

(42) Shimanouchi, T. *NSRDS−NBS* **1972**, *39*.

(43) Jacox, M. E. In *Vibrational and Electronic Energy Levels of Polyatomic Transient Molecules*; Jacox, M. E., Ed.; National Institute of Standards and Technology; Gaithersburg, MD, 1998; Vol. 69, p 945.

(44) Truong, T. N.; Truhlar, D. G. *J. Chem. Phys.* **1990**, *93*, 1761.

(45) (a) Pitzer, K. S.; Gwinn, W. D. *J. Chem. Phys.* **1942**, *10*, 428. (b) Pitzer, K. S. *J. Chem. Phys.* **1946**, *14*, 239. (c) Kilpatrick, J. E.; Pitzer, K. S. *J. Chem. Phys.* **1949**, *11*, 1064. (d) Li, J. C. M.; Pitzer, K. S. *J. Phys. Chem.* **1956**, *60*, 466.

(46) (a) Eckart, C. *Phys. Rev.* **1930**, *35*, 1303. (b) Bell, R. P. *The Tunnel Effect in Chemistry*; Chapman and Hall: New York, 1980.

(47) Brown, R. L. *J. Res. Natl. Bur. Stand. (U.S.)* **1981**, *86*, 357.

(48) (a) Gonzalez, C.; Schlegel, H. B. *J. Chem. Phys.* **1989**, *90*, 2154. (b) Gonzalez, C.; Schlegel, H. B. *J. Phys. Chem.* **1990**, *94*, 5523.

(49) (a) Garret, B. C.; Truhlar, D. G. *J. Phys. Chem.* **1979**, *83*, 2921. (b) Garret, B. C.; Truhlar, D. G. *J. Chem. Phys.* **1984**, *81*, 309. (c) Skodke, R. T.; Garret, B. C.; Truhlar, D. G. *J. Phys. Chem.* **1981**, *85*, 3019. (d) Skodje, R. T.; Garret, B. C.; Truhlar, D. G. *J. Chem. Phys.* **1982**, *77*, 5955. (e) Garret, B. C.; Truhlar, D. G.; Grev, R. S. Magnuson, A. W. *J. Chem. Phys.* **1980**, *84*, 1730. (f) Garret, B. C.; Truhlar, D. G.; Grev, R. S. Magnuson, A. W. *J. Chem. Phys.* **1983**, *87*, 4554.

(50) (a) Miller, W. H.; Shi, S.-h. *J. Chem. Phys.* **1981**, *75*, 2258. (b) Miller, W. H.; Smith, F. T. *Phys. Rev.* **1978**, *A 17*, 939.

(51) Reference 6 and references therein.

(52) The results of these studies will be reported elsewhere.